Front. Struct. Civ. Eng. 2020, 14(4): 867–887
https://doi.org/10.1007/s11709-020-0649-9

RESEARCH ARTICLE

# Typical diseases of a long-span concrete-filled steel tubular arch bridge and their effects on vehicle-induced dynamic response

**Jianling HOU[a], Weibing XU[a*], Yanjiang CHEN[a], Kaida ZHANG[a], Hang SUN[b], Yan LI[b]**

[a] *College of Architecture and Civil Engineering, Beijing University of Technology, Beijing 100124, China*

[b] *School of Transportation Science and Engineering, Harbin Institute of Technology, Harbin 150090, China*

[*] *Corresponding author. E-mail: weibingx@bjut.edu.cn*



**ABSTRACT** A long-span concrete-filled steel tubular (CFST) arch bridge suffers severe vehicle-induced dynamic responses during its service life. However, few quantitative studies have been reported on the typical diseases suffered by such bridges and their effects on vehicle-induced dynamic response. Thus, a series of field tests and theoretical analyses were conducted to study the effects of typical diseases on the vehicle-induced dynamic response of a typical CFST arch bridge. The results show that a support void results in a height difference between both sides of the expansion joint, thus increasing the effect of vehicle impact on the main girder and suspenders. The impact factor of the displacement response of the main girder exceeds the design value. The variation of the suspender force is significant, and the diseases are found to have a greater effect on a shorter suspender. The theoretical analysis results also show that the support void causes an obvious longitudinal displacement of the main girder that is almost as large as the vertical displacement. The support void can also cause significant changes in the vehicle-induced acceleration response, particularly when the supports and steel box girder continue to collide with each other under the vehicle load.

**KEYWORDS** long-span arch bridge, expansion joint disease, vehicle-bridge coupling vibration, dynamic response

## 1 Introduction

The long-span concrete-filled steel tubular (CFST) arch bridge is one of the main types of bridges used in cities and highways [1,2]. It has the advantage of good spanning capacity. A steel box girder is frequently used as the main girder in this type of bridge, which exhibits less stiffness than a conventional concrete arch bridge [3]. Thus, the vehicle-induced dynamic response it exhibits during service is significant. The bridge is prone to numerous diseases due to the effect of vehicles [4].

Owing to the remarkable vehicle-induced dynamic response, various diseases, and a complex stress system [5–7], several relevant studies on this type of bridge have been conducted, primarily comprising field testing and finite element numerical analysis [8–11]. For instance, using field testing and a theoretical analysis, Roeder et al. [12] studied a steel-tied arch bridge with a large vibration response and serious fatigue cracking. The results showed that this type of bridge was flexible and susceptible to large deflections and vibrations caused by vehicles, which was the main reason for the fatigue of its critical components. Huang [13] studied the dynamic characteristics and impact factor (IF) of a half-through CFST bridge and found that the IF of the moments at the arch ends were considerably larger than those at the mid-span for this type of bridge, with span lengths less than or equal to 110 m. Relevant formulas for calculating the IF were then proposed. Zhou and Li [4] studied common diseases affecting a CFST arch bridge. The results showed that the vibration of the CFST bridge, when in service, was remarkable. Several suggestions for the design of a CFST bridge were proposed, encompassing construction, maintenance, and other factors. Wang et al. [14] studied the dynamic response of a CFST cable-stayed arch bridge under vehicles and found that the dynamic IFs vary among different bridge

*Article history: Received Jul 1, 2019; Accepted Oct 14, 2019*

components. Li et al. [15,16] also studied the vehicle–bridge coupling vibration of a CFST arch bridge and found that the IF formula derived from design standards significantly underestimates the effect of dynamic impact, which may have a negative influence on bridge safety. These studies helped clarify the mechanism of the clear dynamic response and various diseases that arise in relation to general design methods.

In recent years, local and comprehensive studies on the vehicle-induced vibration of CFST bridges have become a major area of research. For instance, Haghani et al. [17] studied over 100 fatigue damage cases involving steel and composite bridges and found that more than 90% were deformation-induced and generated by some form of unintentional or otherwise overlooked interaction between different load-carrying members or systems in the bridge. Wu et al. [18] measured the vehicle-induced responses of eight CFST arch bridges to carefully study the IFs of the arch rib and deck. The results showed that a greater impact effect might occur on these components in service and that the local impact effect could not be ignored. Wang and Okumatsu [19] studied the causes of a fractured bolt between the bearing and the girder of a half-through steel-arch bridge and found that axial forces, induced by longitudinal displacements of the girder under vehicles, were the main cause of the observed cracks and bolt fracturing. Shao et al. [20,21] analyzed the impact effect of the suspenders of a through CFST arch bridge using finite element methods. The results indicated that the roughness of the deck had a strong influence on the IF of the suspenders. This factor fluctuated with increasing speed; the dynamic internal force of the suspenders clearly increased with shortening length under the vehicle load. Zhu and Yi [22] also investigated the non-uniformity of the stress IF of suspenders on half-through or through arch bridges under dynamic loading of vehicles using finite element numerical analysis. The results showed that short suspenders were most sensitive to the change in vehicle weight and that simply increasing the structural damping ratio could not reduce the stress IF of the suspender. In addition, scholars have proposed some new methods to analyze the dynamic response of structures or components with time-varying parameters, including methods based on artificial neural networks and deep collocation. These methods can be used to predict the dynamic response of a time-varying system and consider the influence of the disease deterioration [23,24]. These typical research works can also be used for references.

Summarizing the research conducted to date, diseases occur frequently in long-span CFST arch bridges. The vehicle-induced impact effect changes significantly when these diseases occur. However, few quantitative studies of the typical diseases of such bridges and their effects on vehicle-induced dynamic response have been conducted. In this study, a typical long-span CFST arch bridge is taken as a prototype, and the typical diseases that occur in the bridge are systematically investigated and analyzed. The influence of typical diseases on the bridge's basic dynamic characteristics and vehicle-induced dynamic response are explored through a series of field tests and theoretical analyses.

## 2 Prototype bridge

The prototype bridge is a typical three-span CFST arch bridge. The span arrangement is 51 + 158 + 51 m. The layout of the bridge is shown in Fig. 1. The width of the bridge is 27 m. The main span consists of a steel box girder (SB1). The side span consists of a prestressed concrete box girder (CB1 and CB2). The steel box girder is 110.8 m long and the concrete box girder is 74.6 m long. The shape of the steel box girder is consistent with the concrete box girder. The side-span concrete girder extends through the beam-arch joint. It connects the steel box girder at the bracket using a bearing system. The side span is partly supported by a V-shaped structure. The main arch ring is composed of a main arch rib and two stable arch ribs. The connections between the main rib and stable arch ribs are a series of crossbeams. The angle between the stable arch rib plane and the main arch rib plane is 21.8°. To resist the horizontal force of the main arch, six horizontal tie bars are arranged in the central septal zone. There are 16 suspenders on each side of the bridge. The angle between the plane of the suspenders and the horizontal plane is 84°–86°. To distinguish the suspenders, those on the south side are numbered S1–S16 from east to west, and those on the north side are numbered N1–N16. The layout of the bridge is given in Fig. 2. The main girder utilizes a D80 elastomeric flexible strip and a D160 modular expansion joint at the west and east ends, respectively, as shown in Fig. 3.

**Fig. 1** Photograph of the bridge.

The bearing system of the bridge is highly complex. The bearing is located at the bracket between the steel box girder and the concrete box girder. The fixed and unidirectional sliding supports (the vertical supports) are fixed on the east and west sides of the concrete box girder, respectively. The steel box girder is arranged on the supports. The roofs of the supports are welded to the steel

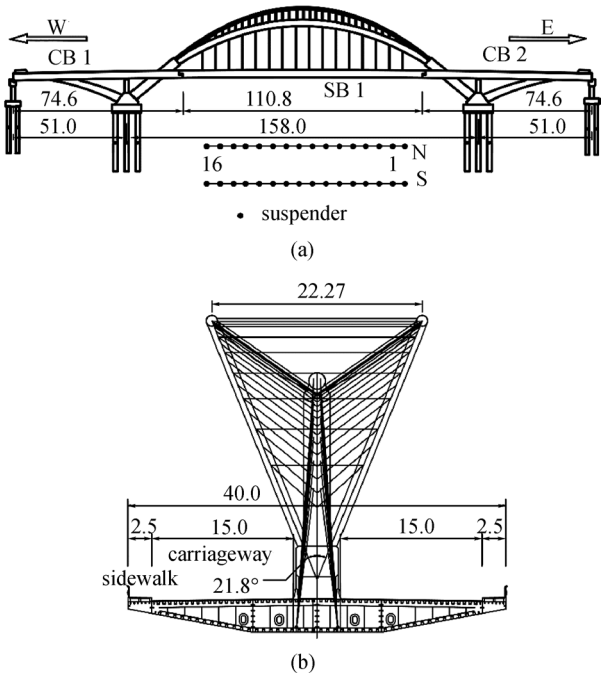


**Fig. 2** Bridge layout (unit: m). (a) Elevation view; (b) side view.

girder, whereas the floors of the supports are bolted to the reserved steel plate on the concrete girder. The vertical supports are all tension-compression spherical. To resist transverse movement, two transverse limit supports are installed on each side of the box girder. The arrangement of the bearing is presented in Fig. 4.

## 3 Analysis of diseases and their effects

### 3.1 Investigation into typical diseases

#### 3.1.1 Disease of the expansion joint

Two types of expansion joint are utilized in this bridge. Through a field investigation, typical diseases of the expansion joint were identified as follows: the rubber sealing strip was blocked; some local cracking and breakage occurred in the anchorage zone; the east-south side crossbeam was partly fractured. A significant height difference was found between both sides of the crossbeams. The typical diseases are shown in Fig. 5.

As Fig. 5 shows, the maximum height difference between the two sides of the expansion joint can reach up to 10 mm without traffic loads. There are obvious bumping phenomena near the bridgehead when vehicles pass through the expansion joints. There was also a significant vertical and longitudinal vibration response in the steel box girder. The height difference between the two sides of the expansion joint (between the steel box girder and the concrete box girder) was substantially amplified by the traffic loads. The authors therefore conducted comprehensive field testing on the relative displacement response between the two sides of the expansion joint. The vehicle-induced dynamic response of the main girder was also tested. The detailed results of these tests are presented in Section 3.2.

#### 3.1.2 Disease of the support

The obvious vehicle-induced dynamic response is primarily caused by the significant height difference between the two sides of the expansion joint [25,26], which in turn is affected by the working state of the supports. The authors therefore conducted a detailed inspection of the supports.

The field investigation results show that the transverse limit supports were in good technical condition. Weld cracking and partial detachment had occurred in the top steel plates of the vertical supports, which therefore cannot provide effective support for the steel box girder. The diseases of the side supports were more serious than those of the middle supports, and the diseases of the south side supports were more serious than those of the north side supports. In addition, several supports also suffered from corrosion of the steel plate, damage to the protective rubber, larger residual deformation, and position deviation. The typical diseases are shown in Fig. 6. It is important to

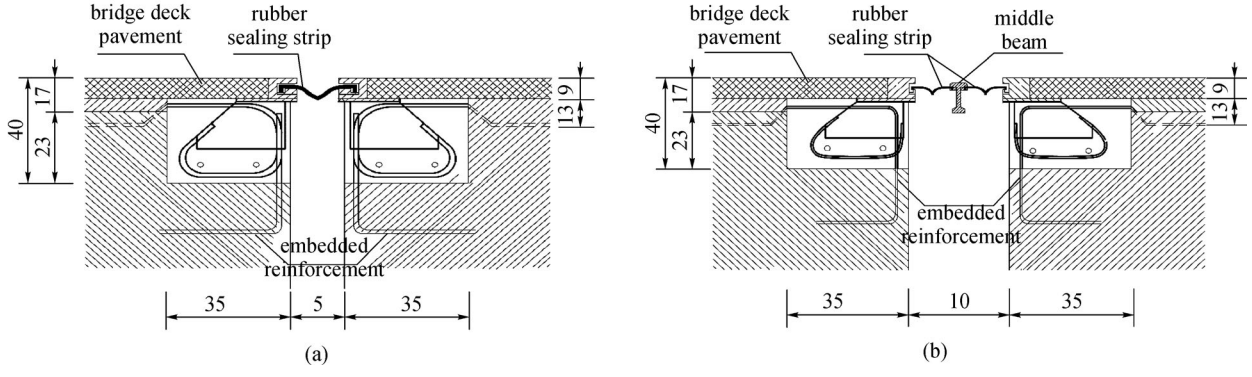


**Fig. 3** Layout of the expansion joint (unit: cm). (a) D80; (b) D160.

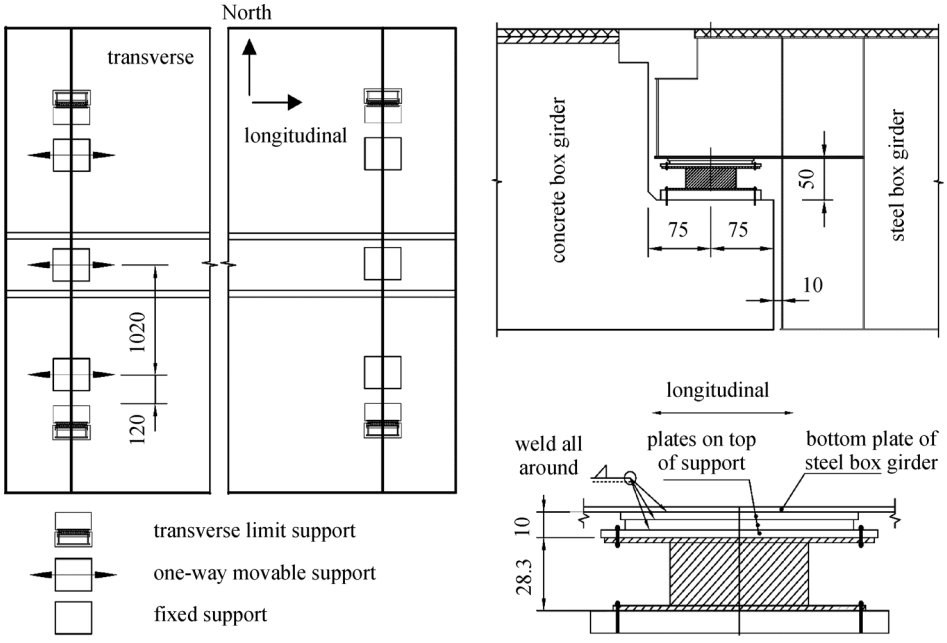


**Fig. 4** Layout of the supports (cm).

(a) (b)

**Fig. 5** Typical disease of the expansion joint. (a) Modular expansion joint (East-South); (b) elastomeric flexible strip (West-South).

note that, because diseases of the side vertical supports can induce a larger rotation response in the steel box girder, they are more dangerous than diseases of the middle supports. Moreover, the rotation of the steel box girder may also aggravate the damage to the side supports.

### 3.1.3 Disease of the suspender

Diseases of the expansion joints and supports can aggravate the vehicle-induced dynamic response. This, along with variations in the boundary condition, may change the stress state of the entire bridge, and particularly the stress state of the suspenders. Diseases of the suspenders may induce collapse and other serious disasters. Therefore, the authors investigated the working state of the suspenders under the closing traffic condition. At present, most of the anchor plates and the suspender nuts suffer from corrosion. There was no obvious abnormal connection damage in the anchorage area on either side of the suspenders. Typical diseases of the suspender are presented in Fig. 7.

To clarify the force of the suspenders, they were tested and analyzed using the frequency method [27,28]. For the articulated boundary of the suspender [29,30], the suspender force $T$ can be determined by Eq. (1).

$$T = \frac{1}{n^2} 4ml^2 f_n^{\,2} - n^2 \pi^2 \frac{EI}{l^2}, \tag{1}$$

where $f_n$ is the $n$th order vibration frequency of the suspender, $m$ is the linear density of the suspender, $l$ is the calculated length of the suspender, $E$ is the elastic modulus of the suspender, and $I$ is the bending inertia of the suspender.

It should be pointed out that the bridge was opened in

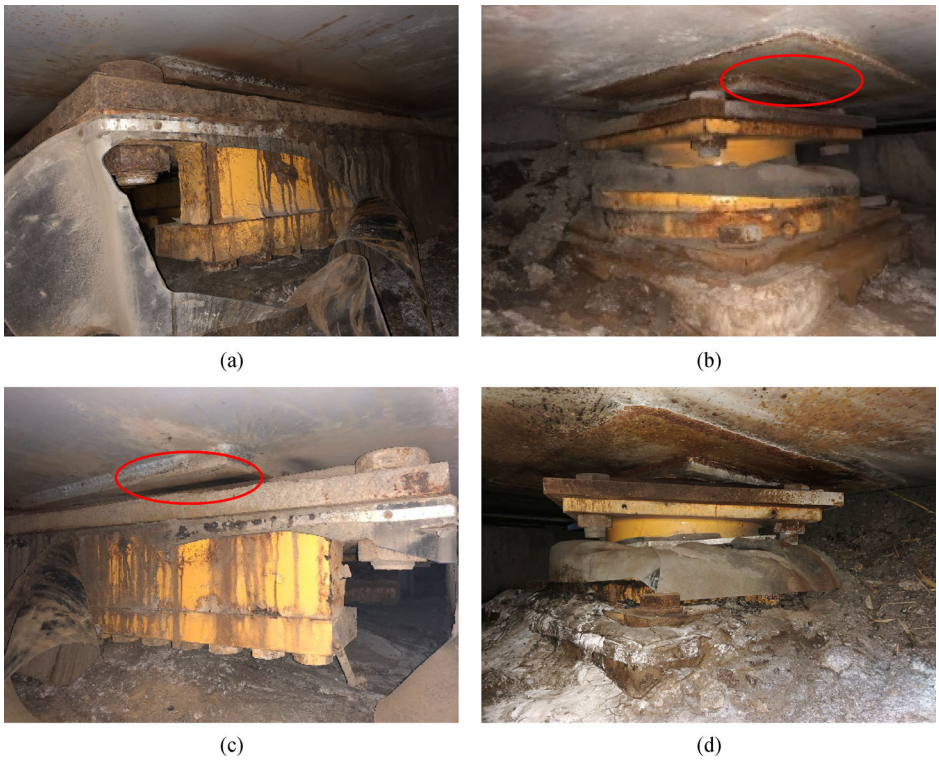


**Fig. 6** Diseases of the steel box girder support. (a) Corrosion of the steel plate (the West middle support); (b) weld cracking and partial detachment (the West-North side support); (c) weld cracking and partial detachment (the West-South side support); (d) larger residual deformation and position deviation (the East-North side support).

**Fig. 7** Disease of the suspender.

November 2009. The authors carried out the acceptance testing of the bridge in June 2010. The dynamic response of the bridge under the vehicles was found to be significantly increased approximately four years later (in 2014). There were obvious relative displacement responses on both sides of the expansion joint. Therefore, the authors carried out a field test of the bridge in July 2014, including basic dynamic parameter testing, suspender force testing, and shape testing of the main arch. According to the test results, the suspender forces had changed significantly. However, the shape of the main arch was consistent with the design shape. There was some relative displacement between two sides of the expansion joints (approximately 10 mm). In this case, the situation of the bridge was tested with a two-year spacing. Table 1 shows the measured suspender force of the bridge without the effect of traffic loads.

As Table 1 shows, compared with the completion stage of the bridge (in 2010), the suspender forces have changed significantly. The maximum increase in the short suspender force is 80.5%. Compared with the total suspender forces in 2010, the total suspender forces increased by approximately 11.1% and 15.0% in 2014 and 2018, respectively. The change trend of the suspender forces is consistent with the development trend of the support diseases. Furthermore, the south side suspender loads differ significantly from the north side suspender loads. The total suspender force of the south suspenders is approximately 15740 kN, whereas that of the north side is approximately 14270 kN. The force of the south suspender is approximately 10% larger than that of the north. For instance, they suffered more loads under a dead load. This phenomenon is consistent with the support condition, in which more serious diseases occurred in the south side supports (as discussed Section 3.1.2). In addition, the total suspender force of the bridge was approximately $3.00 \times 10^4$ kN in 2018, which is almost equal to the total weight of the steel box girder ($3.07 \times 10^4$ kN). The self-weight of the steel box girder was almost borne by the

**Table 1** Measured suspender force without the effect of traffic loads

| suspender | force (kN) | | | suspender | force (kN) | | |
|---|---|---|---|---|---|---|---|
| | 2010 | 2014 | 2018 | | 2010 | 2014 | 2018 |
| s1 | 679.59 | 1058.40 | 1108.22 | n1 | 680.64 | 740.13 | 759.09 |
| s2 | 874.61 | 805.96 | 823.34 | n2 | 874.68 | 805.96 | 797.34 |
| s3 | 886.20 | 820.00 | 765.21 | n3 | 887.08 | 841.37 | 805.38 |
| s4 | 855.56 | 948.24 | 940.50 | n4 | 855.36 | 909.83 | 909.83 |
| s5 | 839.00 | 1080.98 | 1092.93 | n5 | 841.08 | 820.93 | 843.00 |
| s6 | 791.42 | 888.79 | 952.10 | n6 | 793.08 | 845.87 | 905.90 |
| s7 | 807.77 | 867.80 | 928.77 | n7 | 805.44 | 823.78 | 897.30 |
| s8 | 789.73 | 947.43 | 963.82 | n8 | 790.08 | 830.17 | 850.93 |
| s9 | 790.11 | 895.36 | 898.71 | n9 | 791.08 | 880.20 | 947.43 |
| s10 | 806.53 | 867.80 | 870.59 | n10 | 807.44 | 867.80 | 870.59 |
| s11 | 791.48 | 890.07 | 871.50 | n11 | 791.08 | 804.02 | 845.87 |
| s12 | 839.33 | 910.42 | 924.61 | n12 | 840.08 | 992.61 | 1027.51 |
| s13 | 856.85 | 1109.80 | 1155.60 | n13 | 856.36 | 872.21 | 990.61 |
| s14 | 887.28 | 1084.06 | 1106.28 | n14 | 888.08 | 941.63 | 1040.28 |
| s15 | 871.31 | 1036.47 | 1106.18 | n15 | 870.68 | 805.96 | 874.34 |
| s16 | 683.64 | 1150.00 | 1234.17 | n16 | 682.64 | 850.20 | 905.38 |

suspenders. The steel box girder was practically suspended to the arch rib, and the bridge seemed to be a complete floating system. The stress state of the bridge had changed remarkably. Moreover, the south suspender force was quite different from the north suspender force. There was an obvious unbalanced force which makes the steel box girder rotate. The vertical support of the steel box girder was likely to be in void. The vehicle-induced response of the steel box girder may be significant.

It should be noted that the influence of wind loads on long-span bridges cannot be ignored. Wind is also an important factor affecting the dynamic response of vehicle-bridge coupling vibration. In fact, the wind load was taken into account in the design of the bridge. The reference period of the design wind load is 100 years and the basic design wind speed is 35.4 m/s. The main components of the bridge affected by wind load are the steel box girder and the main arch ring. To resist the wind load, the steel box girder of the bridge was designed as a streamlined flat wing, and a transverse limit device was installed on the both sides of the bridge. In this case, the bridge is well suited to resist the wind load when the supports are in good condition. The wind load may cause a difference between the North-South suspender forces and the dynamic response of the main girder when the support is void. However, the transverse limit devices have not failed. The influence of the transverse wind load on the main girder is much smaller. Moreover, the maximum wind speed was approximately 5 m/s on the testing day. The influence of wind load on vehicle-induced dynamic response of the bridge is not obvious.

In summary, diseases of this type of bridge mean that the vertical supports may not provide effective support for the steel box girder; thus, the support might be in void. Diseases of the side supports are more serious than those of the middle supports. A significant height difference can be observed between the two sides of the expansion joint. An obvious unbalanced force may exist to make the steel box girder rotate, and the stress state of the bridge can change significantly, particularly the suspender forces. These diseases will reduce the service life of this bridge [31,32].

### 3.2 Field testing and analysis of disease effects

The typical diseases of the bridge may induce an obvious change in the dynamic response of the steel girder and the suspender forces. To study the effects of these diseases, several field tests were conducted under non-closing traffic conditions.

First, a series of vertical acceleration measurements (denoted as Deck1-A–Deck5-A) were taken at the middle of the main span (Deck1-A), 1/4 section of the main span (Deck2-A), both sides of the expansion joint (the pivot area, Deck3-A and Deck4-A), and the middle of side span (Deck5-A). Vertical displacement measurements were then taken at the middle of the main span (Deck1-D) and the pivot (Deck2-D) area near the expansion joint. Finally, the relative displacement between the two sides of the expansion joint (Deck3-D) was measured. Because diseases of the south side supports were more serious, the measurements were all taken at the south side of the girder near the sidewalk. The acceleration responses of the

suspenders were also tested during normal operation. The layout of the measurement positions is presented in Fig. 8.

### 3.2.1 Basic dynamic characteristics of the main girder

Using the MATLAB platform [33], the frequency spectrum of the measured acceleration response of the main girder was analyzed, the results of which are shown in Fig. 9.

As Fig. 9 shows, the first two orders of the vertical vibration frequencies of the side span are 3.02 and 4.20 Hz. The first two orders of the vertical vibration frequencies of the main span are 0.69 and 1.93 Hz. The vertical vibration frequencies of the steel box girder are considerably smaller than the vibration frequencies of the concrete box girder. This is because the self-weight of the steel box girder was far less than that of the concrete box girder. The vertical bending stiffness of the steel box girder was considerably less than that of the concrete box girder. Thus, deformation between the steel box girder and the concrete box girder will be significantly different under identical vehicle loads. If the supports cannot provide effective support capacity, the difference in deformation between the two sides of the expansion joints will be larger and bumping will frequently occur. Furthermore, the damping ratios can be calculated by the above spectral curves using the half-power point method. Table 2 presents the basic dynamic characteristics of the steel box girder in recent years. The parameters in Table 2 are obtained by the spectral analysis of the vertical acceleration response of the main girder under closing-traffic condition (under environmental excitation).

As Table 2 shows, the natural vibration frequency of the steel box girder decreased as the years of service increased, whereas the damping ratio of the steel box girder first increased and then decreased. It also shows that the diseases affecting the bridge have changed over the years. For example, the supports were in good condition in 2010. The vertical bending stiffness of the steel girder was also relatively large. However, the supports have suffered more damage in recent years, even when in void. The vertical bending stiffness of the steel girder has now become extremely small. According to the test results, the first-order vertical stiffness of the main girder was only 0.95 Hz in 2014. The equivalent vertical stiffness of the main girder was only 51.1% of the designed value (in 2010). In addition, the first-order vertical vibration frequency of the steel box girder was approximately 0.687 Hz in 2018, and the equivalent vertical stiffness of the main girder decreased to 37.0% of the designed value. There may be a significant differential response between the steel girder and the concrete girder that causes the progressive failure of the supports and the expansion joints.

The damping ratios are obtained by the above spectral

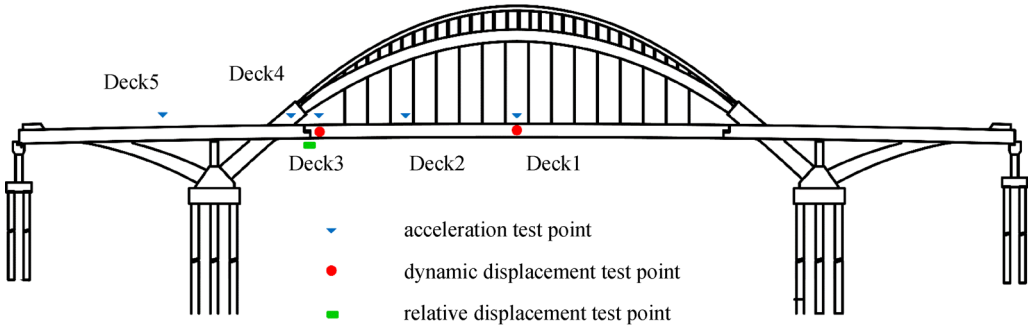


**Fig. 8** Layout of the measurements.

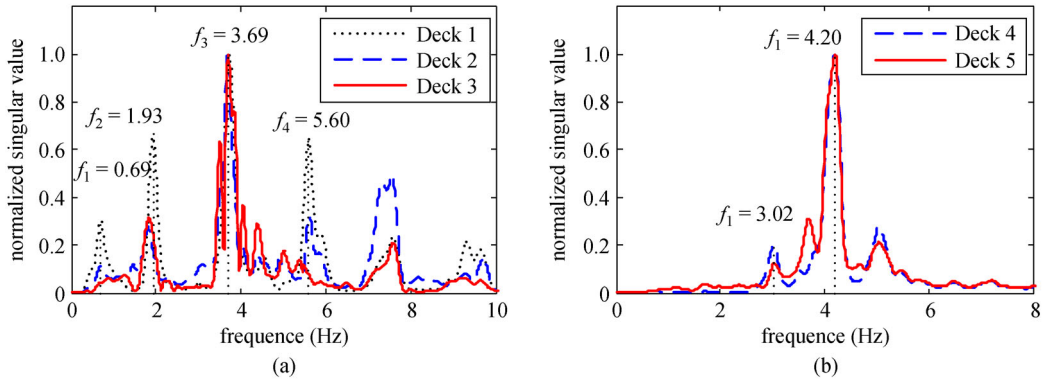


**Fig. 9** Frequency spectrum of the acceleration response of the girders. (a) Steel box girder; (b) concrete box girder.

**Table 2** Dynamic characteristics of the bridge

| testing year | vertical first order | |
|---|---|---|
| | frequency (Hz) | damping ratio (%) |
| 2010 | 1.859 | 3.30 |
| 2014 | 0.950 | 3.87 |
| 2016 | 0.815 | 3.00 |
| 2018 | 0.687 | 1.47 |

curve using the half-power point method, because the modal damping of a structure is related to the variation of its modal parameters. Combined with the field testing results in Section 3.1, the conditions of the supports were essentially the same as the design conditions in 2010. The supports can provide effective tension and compression capacities. The related damping ratio (3.3%) can be approximately regarded as the designed damping ratio of the bridge of the first-order vertical modal. As is well known, the designed damping ratio of a steel structure is approximately 2.0%, and that of a concrete structure is approximately 5.0%. For a CFST arch bridge, the designed damping ratio is between 2.0% and 5.0%. Thus, the measured damping ratio of the bridge in this study is reasonable. In addition, existing studies indicate that the damping ratio tends to increase with damage development in the early stage, which is due to the increasing energy dissipation capacity of structures. However, when the damage accumulates to a certain extent, the interaction between the components of structures is weakened, and the energy dissipation capacity of structures is reduced, such that the damping ratio of the structure tends to decrease [34,35].

Compared with the testing results of the supports, the local cracking or weld damage in the top steel plates of the vertical supports may occur first. The friction between the top steel plates of the supports and the steel box girder increases, and the plastic energy dissipation of the steel plates also increases. Thus, the energy dissipation of the bridge increases, and the damping ratio increases in this case. This phenomenon was found in the comparison between the measurement damping ratio in 2010 and 2014. The increasing proportion of the damping ratio is 17.3%. With the further development of the damage, the interaction between the supports and the main girder becomes weaker. The supporting system of the steel box girder gradually changes from supports to suspenders, and the steel box girder becomes a floating system. Therefore, the damping ratio of the bridge decreases. The maximum reduction ratio of the damping ratio was approximately 55.4% when the damage was aggravated in 2018. It should be noted that through a statistical analysis of the traffic flow in the last decade (2009–2019), the traffic flow of small cars (total weight is less than 20 kN) increased by approximately 15%. However, the composition of the heavy traffic flow is relatively stable, because small cars have significantly weaker effects on the damage development of the bridge (the peak value of the displacement response induced by small cars is usually smaller than 5 mm). Therefore, the development of the disease of the bridge has little relation to the increasing traffic flow.

### 3.2.2 Displacement response of the steel box girder

The field investigation shows obvious vehicle-induced dynamic responses of the steel girder when vehicles pass through the expansion joints. The relative displacement response between the two sides of the expansion joint was tested under non-closing traffic conditions. The traffic flow is relatively large during 07:00–09:00 and 18:00–20:00. Therefore, the authors carried out the field testing of the displacement response of the bridge during 18:00–20:00. Figure 10 presents a typical time-history of the relative displacement response between the two sides of the expansion joint.

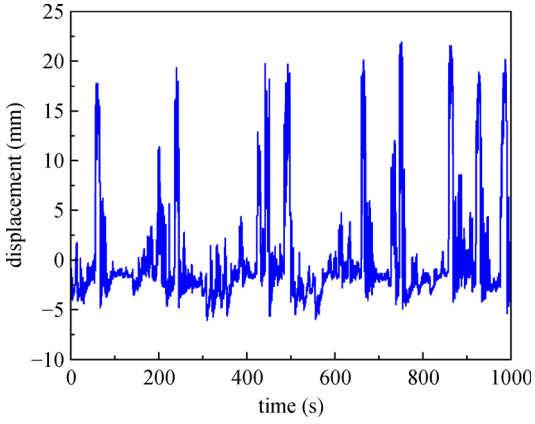


**Fig. 10** Time-history of the relative displacement response between two sides of the expansion joint (Deck3-D).

As Fig. 10 shows, there is a significant relative displacement response between the two sides of the expansion joint under vehicle loads. The peak value of the relative displacement response is 21 mm. The traffic flow over the bridge is significantly large under the non-closed traffic condition. According to the field testing records, the relative displacement amplitude of 10 mm is mainly caused by one heavy truck crossing the bridge along the outside lane (total weight 300 kN, with four-axis), or two medium trucks (total weight 200 kN with three-axis) crossing the bridge side by side along the outside lane. The relative displacement amplitude of 20 mm is mainly caused by several medium or heavy trucks crossing the bridge at the same time, and the relative displacement of 5 mm is always caused by one medium truck or more than 10 small cars (total weight 20 kN with

two-axis) crossing the bridge. The relative displacement amplitude of 2 mm or less is mostly caused by five or fewer small cars. A heavy truck, the total weight of which was more than 300 kN, appeared once in approximately 2 min, and there were four or more trucks crossing the bridge per 3 min during the peak hours, which is essentially consistent with the time interval of the peak relative displacement over 15 mm in Fig. 10. The vehicle-induced displacement responses of the midspan and the pivot were also measured. Figure 11 shows a typical time-history of these responses.

As Fig. 11 shows, the peak values of the displacement response of the midspan and the pivot are 6 and 18 mm, respectively. Contrary to the traditional understanding, the displacement response of the midspan is substantially smaller than that of the pivot. The impact effect of the vehicles is the primary reason for the larger pivot response when the support is in void. To clarify the impact effect of the vehicle on the steel box girder, the IF is calculated using Eq. (2) [36,37].

$$IF = \frac{f_{\mathrm{dmax}}}{\frac{f_{\mathrm{dmax}} + f_{\mathrm{dmin}}}{2}} - 1, \tag{2}$$

where $f_{\mathrm{dmax}}$ is the peak value of the displacement response and $f_{\mathrm{dmin}}$ is the valley value of the displacement response corresponding to $f_{\mathrm{dmax}}$. Based on the test results and Eq. (2), the IF values of the displacement response near the expansion joint and the midspan were 1.52 and 1.15, respectively. Both exceeded the design value of the IF for this type of bridge according to the General Specifications for Design of Highway Bridges and Culverts of China and the Design [38].

In conclusion, the IF values of vehicles change significantly when diseases of supports and expansion joints occur. A significant impact effect will further aggravate the deterioration caused by the diseases. The effects of the diseases on the vehicle-induced dynamic response also need to be considered.

#### 3.2.3 Dynamic response of the suspender

Variation in the vehicle-induced impact effect will have a significant influence on the suspender forces, as the dynamic responses of the suspenders under non-closing loads are non-stationary. The Hilbert-Huang transform (HHT) consists of the empirical mode decomposition (EMD) and the Hilbert spectral analysis (HSA) [39]. The EMD can adaptively decompose signals into finite intrinsic mode functions (IMFs). The instantaneous frequency and Hilbert spectrum of the signals can be obtained by transforming the decomposed IMFs. The HHT is suitable for processing nonlinear and nonstationary signals.

In this study, the HHT method and bandpass filter were used to analyze the dynamic responses of the suspenders [40]. A time-frequency diagram of the suspender was then used to analyze the time-varying suspender forces [41]. The specific method adopted was as follows:

Step 1: Obtain the dynamic response of the suspender.

The acceleration response of the suspender was collected under non-closing traffic conditions. A bandpass filtering method was used to analyze the acceleration response. The first-order modal vibration characteristic of the suspender was then obtained.

Step 2: Decompose the dynamic response of the suspender.

Using the EMD, the dynamic response of the suspender obtained in Step 1 was decomposed into several IMF components and a residual trend item, which can be defined as in Eq. (3).

$$x(t) = \sum_{j=1}^{n} c_j(t) + r_n(t), \tag{3}$$

where $x(t)$ is the original response of the suspender; $c_{j(t)}$ is the $j$th modal function, which is defined as IMF-$j$; and $r_{n(t)}$ is the residual trend item. Based on the above description, the IMFs reflected the components of the original response in different frequency bands. The frequency distributions of $c_{j(t)}$ were arranged in decreasing order.

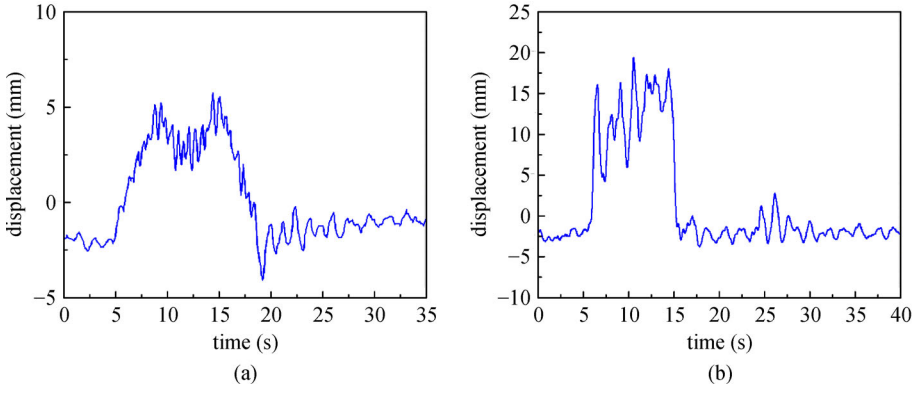


**Fig. 11** Time-history curves of the displacement response of the mid-span and the pivot. (a) Deck1-D; (b) Deck3-D.

Step 3: HHT of IMF.

IMF-1 was processed by HHT following Eq. (4).

$$y(t)=\frac{1}{\pi}p\int_{-\infty}^{\infty}\frac{x(\tau)}{t-\tau}\mathrm{d}\tau, \tag{4}$$

where $p$ is the Cauchy principal value. The transformed signal $z(t)$ was then defined as follows:

$$z(t)=x(t)+\mathrm{i}y(t)=a(t)\mathrm{e}^{i\theta(t)}, \tag{5}$$

where $a(t)$ and $\theta(t)$ are the instantaneous amplitude and phase of the signal, respectively, $i=\sqrt{-1}$, $a(t)=\sqrt{x^2+y^2}$, and $\theta(t)=\tan^{-1}\left(\frac{y}{x}\right)$. The instantaneous frequency of the signal was then determined by Eq. (6).

$$\omega(t)=\frac{\mathrm{d}\theta}{\mathrm{d}t}. \tag{6}$$

By following the above steps, the time-frequency curves of the suspender force were obtained. Based on these, the time-history of the suspender force was calculated using Eq. (1). The mean value of the suspender force was calculated by taking the mean value of the time-frequency curves of the suspender. Thus, the stress amplitude of the suspender force was determined by Eq. (7). The typical time-frequency curves of suspenders S1, S4, and S8 are shown in Fig. 12. To reflect the variation of the suspender forces under the non-closed traffic condition, the authors did not set a special test period, but rather chose an evening rush hour during the testing time of displacement response of the main girder.

$$1+\alpha=\frac{T_{\text{peak value}}}{T_{\text{mean value}}}. \tag{7}$$

As Fig. 12 shows, the time-frequency values of the suspenders change significantly under traffic loads. The suspender force was calculated following Eqs. (2) and (7). In this condition, the stress amplitudes of the suspenders S1, S4, and S8 were in the range of −28.0%–18.5%, −11.9%–18.8%, and −24.3%–17.5%, respectively. The vehicle-induced dynamic response of the suspender force changes significantly after the support void. The shorter suspender is more susceptible to disease. The method introduced in this paper can be used to determine the time-varying characteristic of the suspender force.

It should be noted that the main disease of the bridge is the support void, which causes an increase in the suspender force (the maximum increase ratio is approximately 75%) and an aggravation of the vehicle-induced dynamic response (a large relative displacement on both sides of expansion joints and local damage of expansion joints). However, the stress amplitudes of the suspenders are in the range of 325–525 MPa, which are much less than the ultimate design stress (1395 MPa). Moreover, the shape of the main arch ring is essentially the same as that of the design shape. There is no obvious damage or failure of the

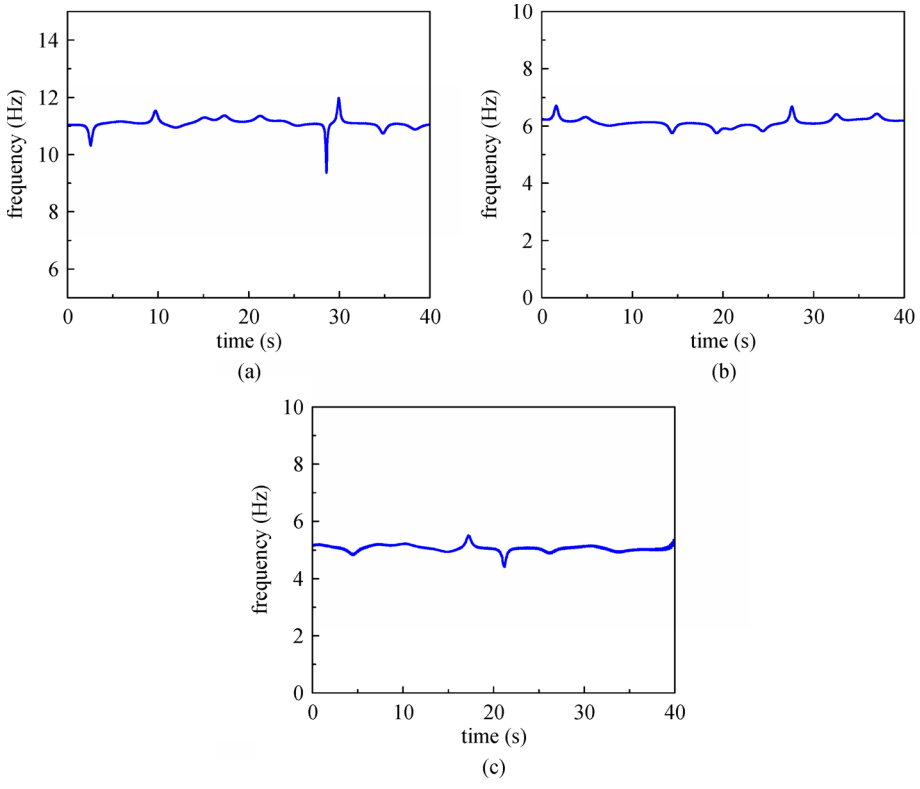


**Fig. 12** Time-frequency curve of suspenders. (a) S1; (b) S4; (c) S8.

main arch ring. In addition, the steel box girder does not have cumulative damage. There are no local welding failures, and the anti-corrosion measures and transverse limit devices of the box girder are still in good condition. In general, the typical diseases have not induced a significant decline in the carrying capacity of the bridge. However, the long-term high stress and local obvious impact effects may lead to a significant reduction in the service life of the bridge. Therefore, the main aim is to clear the influence of the existing diseases on the dynamic response of the bridge, and then provide some suggestions to avoid the diseases' deterioration.

On basis of the field testing results of the bridge, the bridge can still satisfy the basic traffic requirements for the next few years without undergoing repair. However, some suggested methods must be carried out to avoid further diseases, including replacing the supports, adjusting the suspender forces, and increasing the end weight of the steel box girder.

## 4 Theoretical analysis of typical disease effects

As shown in the above analysis, the vehicle-induced dynamic response of the suspender force changes significantly after the support void. However, the influence law of a typical disease on the dynamic response of the prototype bridge is unclear. In this section, the vehicle-induced dynamic response of the prototype bridge is analyzed under different states of disease development.

### 4.1 Component modeling

#### 4.1.1 Superstructure modeling

A three-dimensional finite element model was established using the ANSYS platform. Beam 44 elements were used to simulate the steel box girder, arch ribs, diagonal braces, and transverse braces. Beam 188 elements were used to simulate the V-shaped structure, pre-stressed concrete girder, and column. The section of the main arch rib was a composite CFST section. The yield strength of the steel tube was 345 MPa. The specified compressive strength of the concrete was 50 MPa. The material of the main girder was the same as that of the steel tube. The converted section attributes were calculated to determine the section attributes of the rib beam elements. Link 10 elements simulated the suspenders and the tied bars. The nominal section area of the suspender was 23.48 $cm^2$. The standard strength of the suspender was 1670 MPa. The elastic modulus of the suspender was $1.95\times10^5$ MPa. The realistic properties of the tie bar were the same as those of the suspender. Rigid virtual crossbeams combined both the girder and the suspenders. Thus, the real vertical displacement response of the main girder at the anchorage point was determined as follows:

$$D_n = D_{n0} \pm l_{tn} \cdot \theta, \tag{8}$$

where $D_{n0}$ denotes the vertical displacement response of the beam center, $\theta$ is the twist angle response of the beam, and $l_{tn}$ is the transverse distance between the beam center and the corresponding anchorage point.

#### 4.1.2 Bearing system modeling

Because the transverse limit supports (TLSs) in the bracket were in good condition, an elastic connection was used to simulate the design parameters of the TLSs. The transverse elastic stiffness of the TLSs was $1.0 \times 10^6$ kN/m. However, there are complex diseases of the vertical supports (VSs). The void of the VSs is the main reason for the amplification of the vehicle-induced dynamic response and the change in the stress state of the entire bridge. To simulate the working state of the VS effectively, the gap element was used, as shown in Fig. 13. The method employed to calculate the gap element parameters is shown in Eq. (9).

$$f = \begin{cases} k(d+s), & (d+s \leqslant 0), \\ 0, & (d+s > 0), \end{cases} \tag{9}$$

where $k$ is the elastic stiffness of the gap element, which is equal to the supporting stiffness of the VS ($1 \times 10^6$ kN/m); $s$ is the initial clearance of the gap element, which is equal to zero when there is no void; and $d$ is the relative displacement between the main girder and the support top surface under traffic loads. When the relative displacement between the main girder and the support top surface exceeds the initial clearance, the supporting effects of the VS become clear.

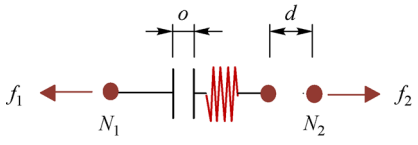


**Fig. 13** Analysis model of gap element.

However, the rigidity of the substructure was significantly larger, and the dynamic response of the substructure was extremely small. The substructure was therefore not considered in the model. The rigidity connections were used to simulate the effects of the substructure. The connection stiffness was $1 \times 10^{10}$ kN/m or $1 \times 10^{10}$ kN/rad. The numerical analysis model of the prototype bridge is presented in Fig. 14.

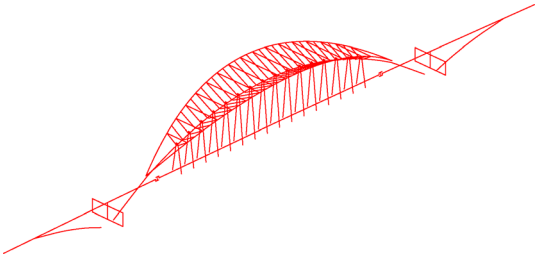

**Fig. 14** Finite element analysis model of the bridge.

#### 4.1.3 Vehicle modeling

A three-axle truck model was adopted for the numerical analysis [42], as shown in Fig. 14(a). The total weight of the truck was 32000 kg. The front axle weight and rear axle weights were 8000 kg (P1) and 12000 kg (P2 and P3), respectively. The longitudinal axle distances were 5.0 m (D1) and 1.6 m (D2), respectively. A triangular load was used to simulate the effects of vehicles on the dynamic response of the bridge, as shown in Fig. 15(b). The load disappeared immediately after action on the model of the girder. The maximum value $F$ was equal to the vehicle axle loads. The loading time $t_0$ was related to the speed of the vehicle, which was determined as follows.

$$t_0 = v_0/l_e, \tag{10}$$

where $v_0$ is the speed of vehicle and $l_e$ is the length of the element of the girder. It should be noted that this study employed a triangular impact load to simulate the vehicle-bridge coupling vibration, which is a simplified method. This method can be used to simulate vehicle-bridge coupling vibration, including the impact effects of vehicles. However, it cannot consider the influence of vehicle parameters and the road roughness on the vehicle-bridge coupling dynamic response. Thus, the interaction force (wheel pressure) between the vehicle and the girder is essentially a constant, as the roughness of the girder is assumed to be in an ideal condition (completely smooth).

#### 4.1.4 Analysis cases

This study focused on the longitudinal and vertical dynamic responses of the steel box girder at the mid-span and the support area under vehicle loads. The dynamic responses of the suspender force were also considered. Four different cases were designed based on typical diseases of the VSs. In more detail, these were as follows.

Case 1: The support was in good condition. The designed parameters of tension and compression stiffness of the supports were applied.

Case 2: A crack in the weld seam between the support and the main girder occurred. The support can only resist compression effects. The gap between the support and the steel box girder was set to 0 mm.

Case 3: The support is in void, but the support and the steel box girder also collided with each other under vehicle loads. Through a trail calculation, the gap was set to 3 mm.

Case 4: The support is completely void. The support and the steel box girder cannot contact each other under vehicle loads. Through a trail calculation, the gap was set to 20 mm.

#### 4.1.5 Method certification

On the basis of the field testing results of actual vehicles crossing the bridge, the dynamic responses of the bridge are quite small under the small cars and light trucks. Thus, the authors chose a heavy truck, the total weight of which was 320 kN, as an example in the numerical analysis process. The center line and side line of the steel box girder were taken as the measurement points in the comparative analysis, as shown in Fig. 16.

The traffic flow field test results showed that two heavy parallel vehicles (where the total weight of each vehicle was approximately 300 kN) would induce a larger dynamic response of the bridge. As a comparative analysis, a single vehicle and two parallel vehicles were considered in the numerical analysis. The support is considered to be

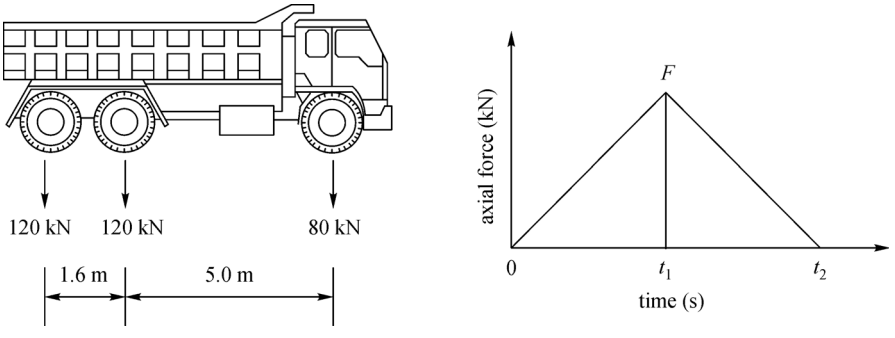


**Fig. 15** Model of vehicle.

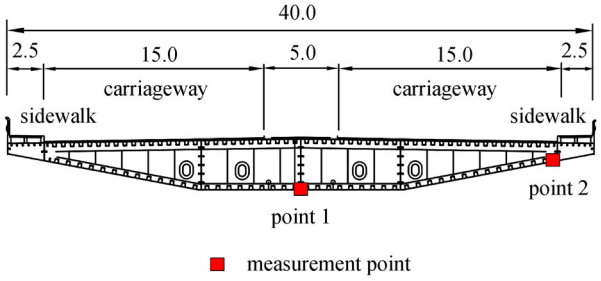


**Fig. 16** Measurement points (unit: m).

completely void. Figure 17(a) gives the time-history of the displacement response of point 1 (VDR-S-1) and point 2 (VDR-S-2) under a single vehicle crossing the bridge along the outermost lane. Figure 17(b) gives the corresponding time-history of the displacement response of points 1 and 2 under two parallel vehicles along the outermost two lanes.

As Fig. 17 shows, the peak displacements of VDR-S-2 and VDR-S-1 are 8.3 and 6.6 mm under a single vehicle, respectively. The peak displacements of VDR-S-2 and VDR-S-1 are 21.2 and 18.2 mm under two parallel vehicles, respectively. Compared with Fig. 10, the numerical analysis results of VDR-S-2 are essentially the same as the field testing results under a single vehicle (10 mm) and two parallel vehicles (22 mm). Because of the influence of additional vehicles, the field testing results are larger than the numerical analysis results.

According to the comparison between the field testing results and the numerical results, the theoretical analysis method can be used to simulate the vehicle-bridge coupling dynamic response. Because the actual situation of the supports is highly complex, and the spatial distribution of the support conditions has significant effects on the vehicle-bridge coupling dynamic response, the authors have not studied the influence of the support condition variations on the vehicle-bridge coupling dynamic response. The uniform spatial distribution of supports is considered during the numerical analysis, and the center point of the steel box girder was chosen as the measurement point (which is less affected by the spatial variation of the support conditions) in the following study.

It should be noted that because the dynamic response of the actual bridge in service is affected by many uncertainties, such as uncertain boundaries and uncertain loads (wind load, random traffic load and so on). In recent findings, the random analysis, the fuzzy analysis, the interval analysis, some neural network and deep energy methods have been proposed to solve the uncertainties of dynamic responses of structures [23,24]. These methods can be used in the further study on vehicle-bridge coupling vibration in consideration of diseases influence.

#### 4.1.6 Damping ratio

At present, the most widely used damping model is still the proportional damping model (classical damping model). A general method to consider the damping variation is to use a nonlinear property component or a nonlinear link member. This method can be used to consider the change in damping after a structural damage. However, the reason for the damping variation (shown in Table 2) of the bridge includes not only the influence of the material nonlinearity of the supports and girder, but also the change in the physical boundary conditions. The damping vibration is difficult to achieve numerically.

Moreover, the nonlinear process mainly includes the nonlinear contact between the supports and the steel box girder. The plastic damage on the contact surface between the supports and the steel box girder is relatively small under the existing vehicle loads according to the inspection results of the field testing. The contact between the supports and the steel box girder is essentially elastic collision. After the supports have completely failed, the structural support system changes. In this case, the components of the new system do not have new nonlinear

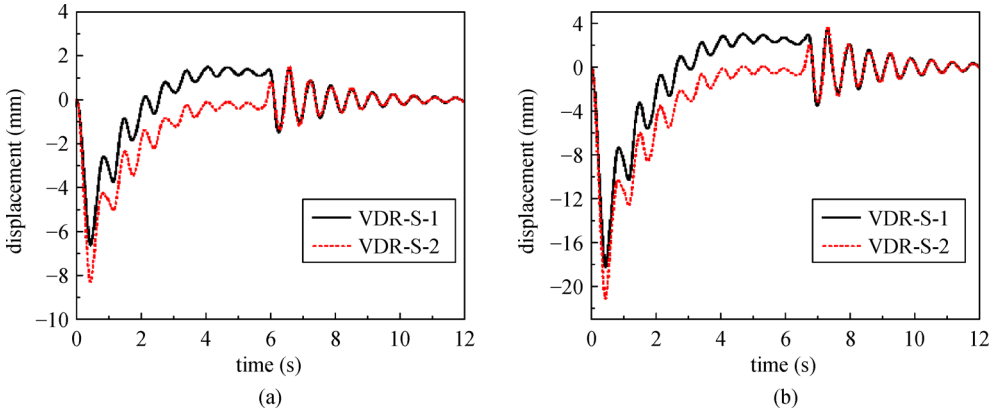


**Fig. 17** The displacement time-history curves. (a) Single vehicle; (b) parallel vehicles.

members to affect the damping of the bridge. Therefore, the damping vibration caused by the nonlinear contact between the supports and the steel box girder was ignored in the numerical analysis. The authors used the measured mode damping ratio to consider the damping variation. Actually, it is a hot topic to construct the relationship between local damage and overall damping variation of structures. It is also a front study to propose a new method to predict damping variation of structural damage.

#### 4.1.7 Numerical speed

The design speed of the bridge is 60 km/h The average speed of traffic flow reduced (almost 20–30 km/h) when the traffic flow was relatively large during the field testing, whereas the average speed of traffic flow increased (even up to 80 km/h) when the traffic flow was low. Therefore, the numerical speed was adjusted to 20, 40, 60, and 80 km/h. In fact, the relationship between average speed of traffic flow and resonance responses of bridges are an interesting study aspect. Vehicle-induced resonance responses of bridges are related to the composition of traffic flow. The responses may affect by the composition parameters of traffic flow, such as stiffness, mass, and suspension system damping.

### 4.2 Dynamic response of the steel box girder in the mid-span

Because the transverse limit supports were in good condition, the transverse dynamic response of the bridge was relatively small. The vertical and longitudinal dynamic responses of the steel box girder were then investigated.

#### 4.2.1 Vertical

Figure 18 gives the time-history curves for vertical displacement response of the steel box girder in the mid-span (VDR-M) under different cases.

As Fig. 18 shows, the VDR-M is greatly affected by the vehicle velocity and the state of the supports. The peak value of the VDR-M increases only slightly with a low velocity. However, the peak value of the VDR-M significantly increases when the velocity reaches 80 km/h Furthermore, the disturbance of the VDR-M increases as the velocity increases and the disease state deteriorates. Figure 19 compares the peak value of VDR-M and vertical acceleration response of the steel box girder in mid-span (VAR-M) under different cases.

As Fig. 19 shows, the dynamic response of the mid-span girder increases as the velocity of the vehicle increases.

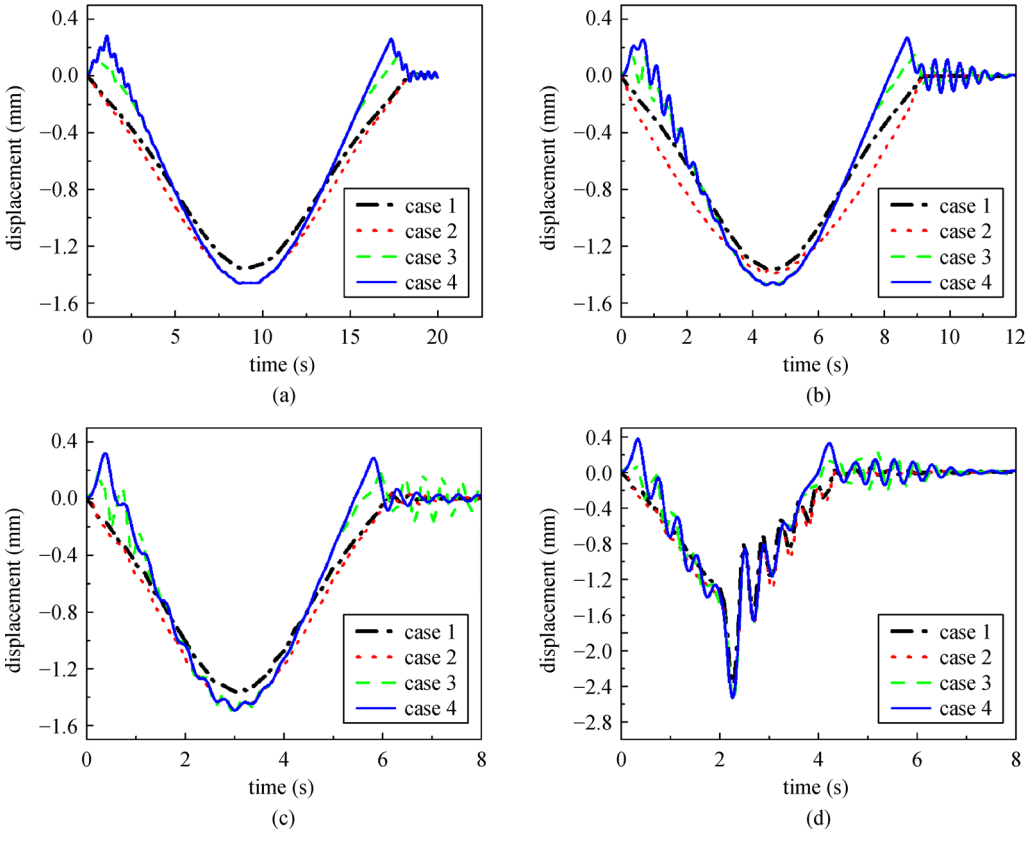


**Fig. 18** Vertical displacement response of the steel box girder in mid-span. (a) 20 km/h; (b) 40 km/h; (c) 60 km/h; (d) 80 km/h.

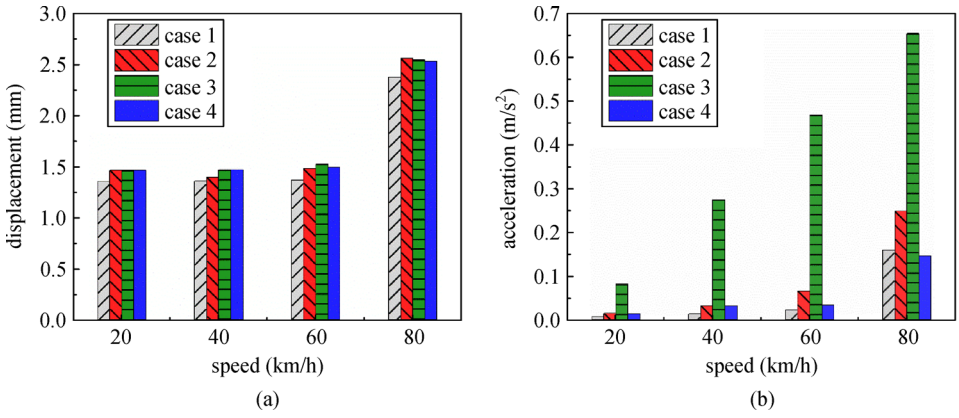


**Fig. 19** Peak vertical dynamic response of the steel box girder in mid-span. (a) Vertical displacement; (b) vertical acceleration.

The disease condition has a significant effect on the vertical dynamic response of the steel box girder. The peak VDR-M first increases and then tends to stabilize as the disease deteriorates. For the numerical cases, the increment of the peak VDR-M reaches 7.2% when the support is void. However, the disease deterioration has a greater effect on the VAR-M. The peak VAR-M first increases and then decreases. The peak VAR-M is considerably larger when the steel box girder is able to collide with the top surface of the supports (case 3). The increment of peak VAR-M reaches 308%. This is because the pounding between the steel box girder and the top surface of the supports has a greater effect on the VDR-M of the mid-span and a smaller effect on the VAR-M of the mid-span.

#### 4.2.2 Longitudinal

Figure 20 gives the time-history curves for the longitudinal displacement response of the steel box girder in the mid-span (LDR-M) under different cases.

As Fig. 20 shows, there is almost no longitudinal displacement response in case 1 under traffic loads. However, the LDR-M of the other cases is significantly larger than that of case 1 under traffic loads. The LDR-M increases as the vehicle velocity increases. The peak LDR-M of case 4 is 1.3 mm when the velocity is 80 km/h, which is of the same order as the peak VDR-M. Figure 21 compares the peak LDR-M and longitudinal acceleration response of the steel box girder in the mid-span (LAR-M) under different cases.

As Fig. 21 shows, the disease condition and the vehicle velocity has significant effects on the longitudinal dynamic response of the steel box girder. The peak LDR-M and LAR-M all increase as the vehicle velocity increases. The peak LDR-M reaches 1.27 mm under traffic loads when the supports are void. The peak LAR-M is 0.15 m/s$^2$. The influence law of the disease conditions on the LAR-M is the same as that on the VAR-M. However, the influence law of the disease conditions on the LDR-M is substantially different from that on the VDR-M. The LDR-M increases as the diseases deteriorate, whereas the peak VDR-M increases and then stabilizes. The reason for this is that, when the supports are void, the suspender can provide effective vertical support for the girder but cannot provide effective longitudinal support for the girder.

### 4.3 Dynamic response of the steel box girder near the support area

Figure 22 shows the time-history curves for the vertical displacement response of the steel box girder near the support area (VDR-S) under different cases.

As Fig. 22 shows, there is almost no VDR-S for case 1 and case 2, owing to the limited displacement of the supports. The peak VDR-S is 3 mm, where there is an initial 3 mm clearance between the steel box girder and the supports for case 3. There is pounding between the girder and the supports when the relative displacement reaches 3 mm. This results in the phenomenon of peak-cutting in the time-history curves of the VDR-S. The maximum VDR-S can reach 7 mm when the support is completely void for case 4 under the numerical condition. It should be pointed out that there are significant oscillations induced in Figs. 18 and 22. Actually, oscillations can also been found when heavy vehicles crosses the bridge during the field-testing. The oscillation amplitude shows the impact effects of vehicles at different locations. The oscillation amplitude of displacement responses can be used to calculate the IFs of vehicles on bridges. The magnitude of IF represents impact effects of vehicles on bridges, as well as effects of vehicles on the safety and durability of bridges. Lager IFs will induce greater stress amplitude of bridge members, lower safety and shorter fatigue life.

Notably, the longitudinal displacement response of the steel box girder near the support area is similar to the LDR-M (see analysis in Section 4.2.2). Figure 23 compares the vertical and the longitudinal acceleration response of the steel box girder near the support area (VAR-S and LAR-S).

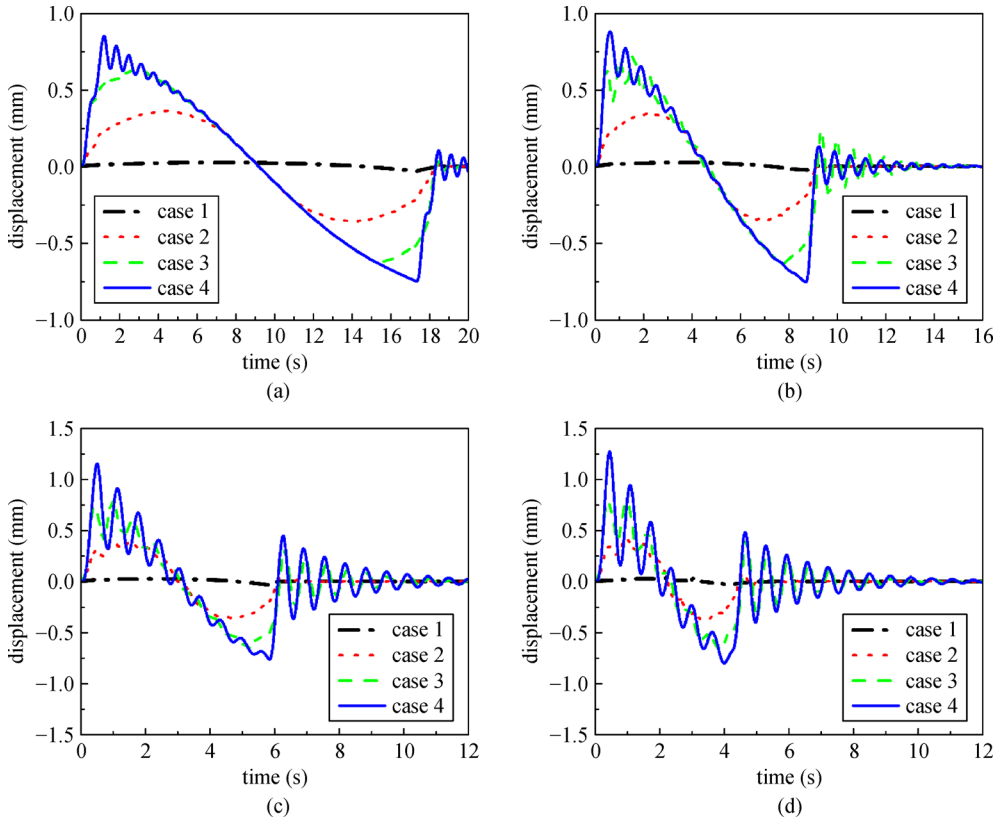


**Fig. 20** Longitudinal displacement response of the steel box girder in mid-span. (a) 20 km/h; (b) 40 km/h; (c) 60 km/h; (d) 80 km/h.

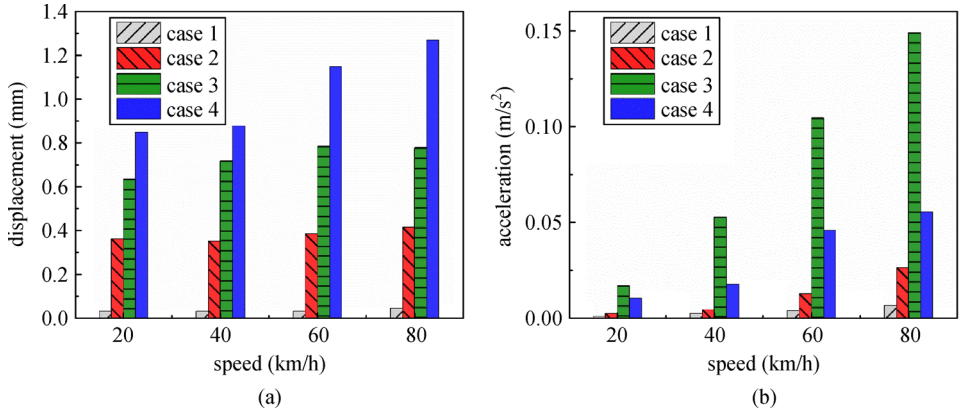


**Fig. 21** Peak longitudinal acceleration of the steel box girder in mid-span. (a) Longitudinal displacement; (b) longitudinal acceleration.

As shown in Fig. 23, the influence laws of the disease deterioration on the VAR-S and LAR-S are similar to those on the VAR-M and LAR-M, respectively. The VAR-S and LAR-S first increase and then decrease as the disease deteriorates. The peak VAR-S of case 3 is 8.3 m/s$^2$, which is considerably larger than those of the other cases. The peak LAR-S is only 0.73 m/s$^2$, which is considerably smaller than that of the VAR-S. This is because the pounding between the steel box girder and the top surface of the supports mostly occurred in a vertical direction. It must be noted that deformation between the steel box girder and the concrete box girder is significantly different under identical vehicle loads; the deformation of the concrete box girder is relatively small. If the supports cannot provide effective support capacity, the difference in deformation between the two sides of the expansion joints will be larger and bumping will occur frequently.

### 4.4 Dynamic response of the suspender force

In this section, the shortest suspender (S1) near the supports and the longest suspender (S8) in the mid-span

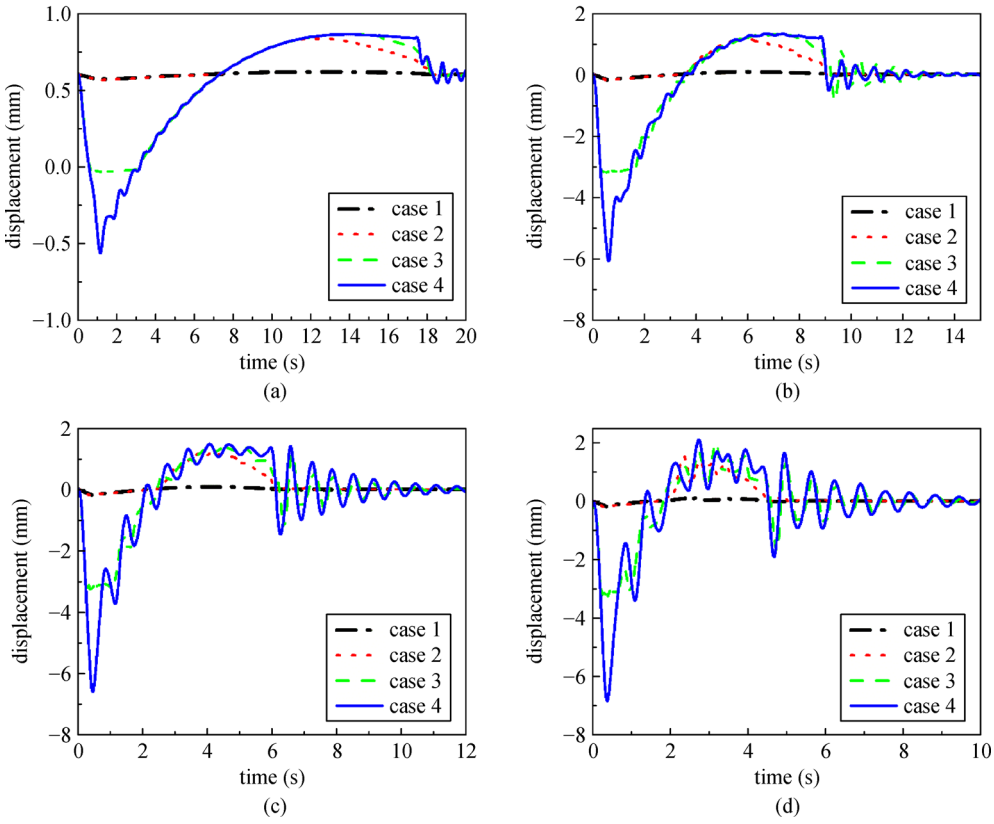


**Fig. 22** Vertical dynamic response of the main beam near the support area. (a) 20 km/h; (b) 40 km/h; (c) 60 km/h; (d) 80 km/h.

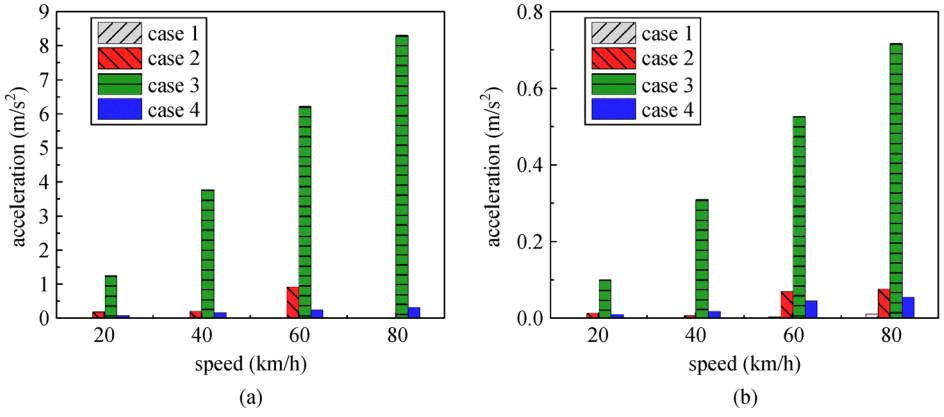


**Fig. 23** Peak acceleration of the steel box girder near the support area. (a) Vertical acceleration; (b) longitudinal acceleration.

are presented as examples. Figure 24 shows the time-history curves of the stress amplitude (SA) of S1 and S8 under different cases with a vehicle velocity of 80 km/h.

As Fig. 24 shows, the disease deterioration has a greater effect on the dynamic response of the suspender force. The variation in the SA increases as the disease deteriorates. The SA of S1 exceeds 7.3% and the SA of S8 exceeds 3.3%. The disease has a greater effect on the SA of the short suspender than on the SA of the long suspender. Figure 25 presents the peak stress amplitude of S1 and S8 under different cases.

As shown in Fig. 25, the peak SA of S1 and S8 both increase as the vehicle velocity increases. The peak SA of S8 first increases and then tends to stabilize. The peak SA of S1 increases as the disease deteriorates. The disease has a greater effect on the SA of the short suspender than on the SA of the long suspender. Moreover, the peak SA of the suspenders does not vary significantly when the disease is not serious (case 1 and case 2). The SA of S1 (1.2%) is smaller than that of S8 (2.0%) in these two cases. However, the SA of S1 is almost twice as large as that of S8 under case 3 and case 4. Thus, disease deterioration has a greater

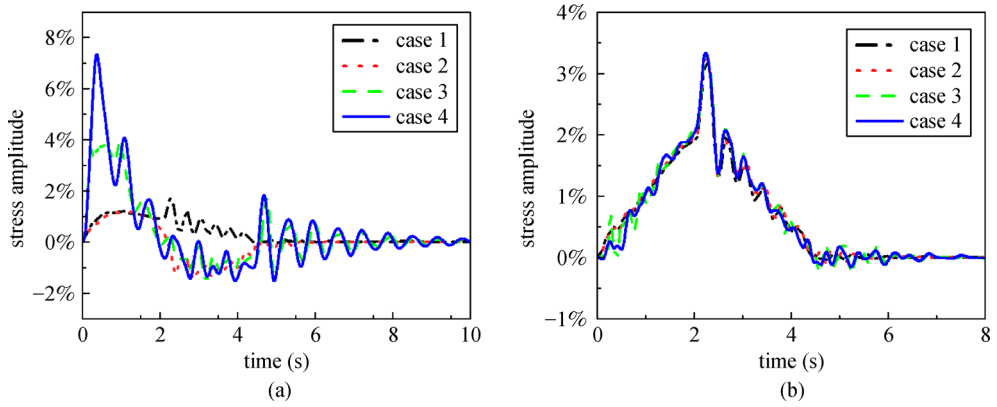


**Fig. 24** Time-history curves for stress amplitude of suspenders. (a) S1; (b) S8.

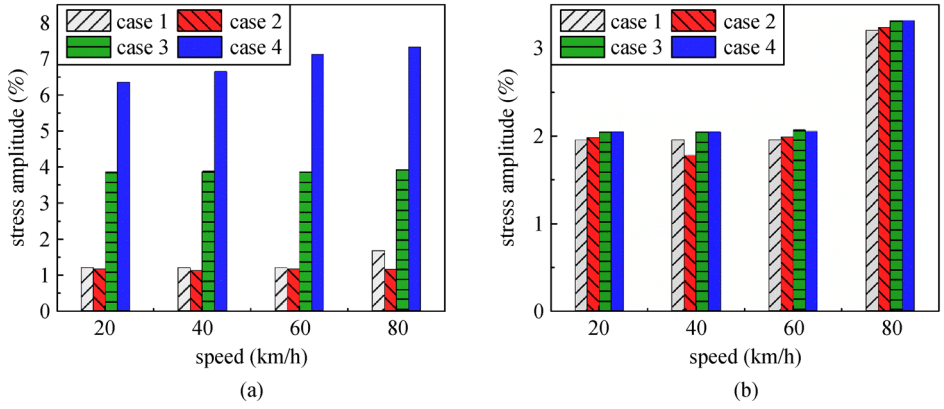


**Fig. 25** Peak stress amplitude of suspenders. (a) S1; (b) S8.

effect on the SA of the short suspender than on the SA of the long suspender.

### 4.5 Supplemental analysis of vehicle following condition

Because the phenomena of vehicle following and vehicle paralleling often occurred during the field testing, the authors included some numerical analysis results of the dynamic response of the bridge under vehicle following conditions. Owing to space limitations, Fig. 26 presents the typical dynamic response results of the bridge under the conditions of three-vehicle following at a speed of 60 km/h.

As Fig. 26 shows, the displacement response of the bridge is more significant under vehicle following conditions. The peak value of the vertical displacement of the mid-span increases approximately 43.1%. The vibration law of the peak acceleration response is consistent with that under a single vehicle. The acceleration response is much larger when the top plate of the support can also collide with the bottom plate of the steel box girder. It should be pointed out that when the second vehicle and the third vehicle begin to cross the main bridge (the relevant times are 2.2 and 4.4 s), the vertical displacement in the mid-span decreases by approximately 14.8% under case 3 and case 4. The reason for this may be that the supports cannot provide an effective support force, and the steel box girder can be regarded as a continuous beam supported by the suspenders. However, in general, the dynamic response law of the bridge under multiple vehicles did not change with the deterioration of the support diseases.

In addition, the recent findings show that the cyclic loads of vehicles can induce damage and cracking of weld joints of supports. This can cause local stress concentration and fatigue failure of steel plates of the supports and girder. It also can increase the stress amplitude of the suspenders and induce local damage of the anchor zone of the suspenders. According to the analysis results of this study, the relative displacement between the main girder and the side girder increases when the supports are damaged, which induces a significant IF of vehicles on the displacement response of the main girder. Moreover, it will cause a high stress of the suspenders, especially the short suspender. The stress amplitude of the short suspender under the field testing cases is between −15% and 20%, and is 7% in the numerical analysis cases (one vehicle). The disease of the support causes a significant short-term effect of vehicles on

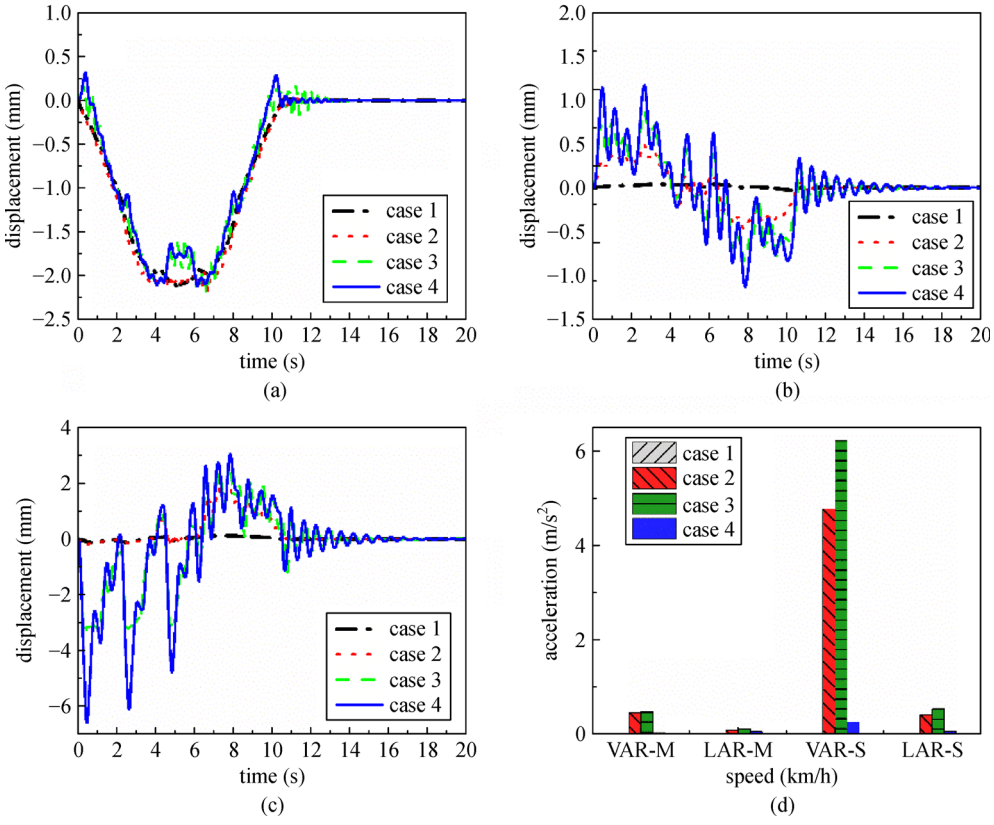


**Fig. 26** Typical dynamic response results of the bridge under three-vehicle following condition at a speed of 60 km/h. (a) Vertical displacement in the midspan; (b) longitudinal displacement in the mid-span; (c) vertical displacement of area near the support; (d) peak acceleration response of the main girder.

the bridge. The displacement responses, acceleration responses, and force responses are all related to the stress state of the bridge. The variation in these parameters also indicates that the dynamic load of vehicles on the bridge component increases. When this short-term effect accumulates over a long period of time, it results in increased damage possibility of the bridge members. Taking the contact forces between the support and the girder as an example, the average contact forces between the support and the girder are shown in Fig. 27.

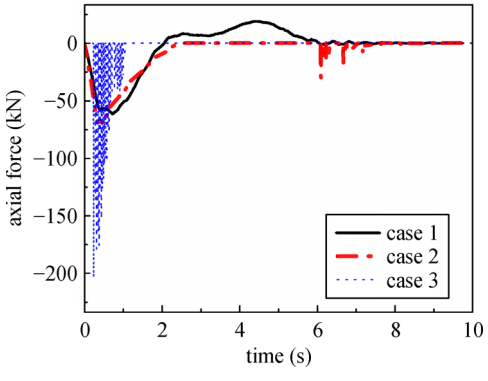


**Fig. 27** Average contact forces between the support and the girder.

As Fig. 27 shows, the contact force between the support and the steel box girder changes significantly as the support disease deteriorates. The supports can provide effective tensile and compressive capacities in case 1, and the average contact force between the support and the steel box girder is approximately 61 kN. However, the relevant contact force is up to 204 kN in case 3, which is 3.3 times as large as that of case 1. According to the change process of the above contact force, it can be concluded that the dynamic responses of bridge components significantly change because of the diseases, which may lead to fatigue and other damage under long-term cumulative action.

It should be pointed out that because the main aim of this study is to clarify the influence of existing damage and its development on the dynamic response of vehicle-bridge coupling vibration, including the change in the dynamic response law of the girder and suspenders, the authors aim to further analyze the existing damage deterioration and the occurrence of new damage induced the existing disease, and then provide guidance for the maintenance and reinforcement of bridges. However, the authors have ignored the hysteresis effect and fatigue accumulation, which would lead to an underestimation of the effects of vehicle loads, and affect the accuracy of our fatigue life assessment of bridge components; these aspects must be addressed in future research.

## 5 Conclusions

This study aimed to clarify typical diseases of a long-span CFST arch bridge and their effects on the vehicle-induced dynamic response of the bridge. Using a typical long-span CFST arch bridge as an example, a series of field tests were conducted. Based on the results, a theoretical model was constructed, and four disease cases were designed. Several numerical analyses were then undertaken to study the effects of the diseases on the vehicle-induced dynamic response of the bridge. The results show that.

1) The relative displacement response between the steel box girder and the concrete box girder is significant when the support is void. The relative displacement response amplitude reaches 21 mm under normal operation conditions. The displacement IF values of the steel box girder near the support and the mid-span were 1.52 and 1.15, respectively. The stress amplitudes of the suspender force were in the range of −28.0%–18.8% and the shorter suspender was more susceptible to the diseases. The HHT method introduced in this paper can be used to determine the time-varying characteristic of the suspender force.

2) The disease condition has a greater effect on the vehicle-induced dynamic response of the CFST bridge. In the numerical cases, the peak VDR-M first increases and then tends to stabilize as the disease deteriorates. The increment in the peak VDR-M in the mid-span reaches 7.2% when the support is void. The LDR-M continues to increase as the diseases deteriorate. The peak LDR-M is 1.27 mm, which is of the same order of magnitude as the VDR-M. Disease deterioration has a greater effect on the VAR-M and LAR-M. The peak VAR-M and LAR-M first increase and then decrease. The peak VAR-M is considerably larger when the steel box girder collides with the top surface of the supports (case 3). The influence law of the disease conditions on the LDR-M is notably different from that on the VDR-M, because the suspender can provide effective vertical support for the girder.

3) Disease deterioration has a far greater effect on the VDR-S, VAR-S, and LAR-S. There is pounding between the steel box girder and the top surface of the supports when the relative displacement reaches the initial clearance between the girder and the supports. Thus, when the pounding occurs, the phenomenon of peak-cutting can be observed in the time-history curves of the VDR-S. The VAR-S and LAR-S first increase and then decrease as the disease deteriorates. The peak LAR-S is considerably smaller than the VAR-S, because the pounding mostly takes place in a vertical direction.

4) The peak SA of S1 and S8 increases as the vehicle velocity increases. The peak SA of S8 first increases and then tends to stabilize. The peak SA of S1 increases as the disease deteriorates. The disease has a greater effect on the SA of the short suspender than on the SA of the long suspender. Moreover, the peak SA of the suspenders does not vary significantly when the disease is not serious (case 1 and case 2). The SA of S1 (1.2%) is smaller than that of S8 (2.0%) in these two cases. However, disease deterioration has a far greater effect on the SA of the short suspender than on the SA of the long suspender, as the SA of S1 is almost twice as large as that of S8.

5) The stiffness difference between the steel box girder and concrete box girder for long-span CFST arch bridges is large. There is a significant difference in deformation between these two types of girder under vehicle loads. This large difference can easily induce diseases in the bearing systems. Once a disease arises in the bridge supports, the vertical and longitudinal dynamic responses of the main girder vary significantly, and the stress amplitude of the suspenders also changes substantially. Consequently, the vehicle-induced dynamic response is generally aggravated, especially when the supports are void. In this case, the vehicle-induced IF of the dynamic response may greatly exceed the guidance provided by the design codes.

**Acknowledgements** This research was supported by the National Natural Science Foundation of China (Grant Nos. 51908015, 51978021), National Key Research and Development Program of China (Grant Nos. 2017YFC1500604, 2017YFC1500603), Beijing Municipal Education Commission (Nos. KM201910005020, IDHT20190504), and the Basic Research Fund of Beijing University of Technology (No. 004000546318524).

## References

1. Chen B C, Wang T L, Asce M. Overview of concrete filled steel tube arch bridges in China. Practice Periodical on Structural Design and Construction, 2009, 14(2): 70–80
2. Zheng J, Wang J. Concrete-filled steel tube arch bridges in China. Engineering (Beijing), 2018, 4(1): 143–155
3. Okamoto Y, Nakamura S, Tanaka H, Moriya Y. Study on steel box girder bridges partly stiffened by CFT arch ribs. Journal of Constructional Steel Research, 2012, 2012(70): 28–35
4. Zhou S, Li W. Causes of common diseases of CFST arch bridge. Journal of Chongqing Jiaotong University (Natural Science), 2013, Sup1(32): 738–741
5. Huo X, Pu Q. Impact factors of butterfly-shaped arch bridges. Journal of Vibration and Shock, 2014, 33(1): 176–182
6. Kang H J, Zhao Y Y, Zhu H P, Jin Y X. Static behavior of a new type of cable-arch bridge. Journal of Constructional Steel Research, 2013, 81(2): 1–10
7. Klein P, Yamout M. Cable-stayed arch bridges, Putrajaya, Kuala Lumpur, Malaysia. Structural Engineering International, 2003, 3(13): 196–199
8. Deng L, Yu Y, Zou Q, Cai C S. State-of-the-art review of dynamic impact factors of highway bridges. Journal of Bridge Engineering, 2015, 20(5): 04014080
9. Deng L, Cai C S. Development of dynamic impact factor for performance evaluation of existing multi-girder concrete bridges. Engineering Structures, 2010, 32(1): 21–31
10. Liu J, Li Y. Development and challenge of the vehicle and highway

bridges dynamic interaction. Key Engineering Materials, 2014, 2014(574): 135–150
11. Yoshimura M, Wu Q. Vibration analysis of the second saikai bridge—A concrete filled tubular (CFT) arch bridge. Journal of Sound and Vibration, 2006, 290(1–2): 388–409
12. Roeder C W, MacRae G, Crocker P. Dynamic response and fatigue of steel tied arch bridge. Journal of Aerospace Engineering, 2000, 5(1): 14–21
13. Huang D. Dynamic and impact behavior of half-through arch bridges. Journal of Bridge Engineering, 2005, 10(133–141
14. Wang W, Yan W, Deng L. Dynamic analysis of a cable-stayed concrete-filled steel tube arch bridge under vehicle loading. Journal of Bridge Engineering, 2015, 20(5): 04014082
15. Li Y, Cai C S, Liu Y, Chen Y. Dynamic analysis of a large span specially shaped hybrid girder bridge with concrete-filled steel tube arches. Engineering Structures, 2016, 2016(106): 243–260
16. Li Y, Zhang W, Liu Y. A method based on meta-model for updating the finite element model of bridges using the measured static and dynamic data. In: The 12th COTA International Conference of Transportation Professionals. Beijing: CICTP, 2012
17. Haghani R, Al-Emrani M, Heshmati M. Fatigue-prone details in steel bridges. Buildings, 2012, 2(4): 456–476
18. Wu Q X, Huang W K, Chen B C. Vehicle-induced vibration research and dynamic analysis for concrete-filled steel tubular arch bridges. Engineering Mechanics, 2013, 30(1): 147–155
19. Wang Q, Okumatsu T. Fatigue failure analysis of cracks near the sole plate of a half-through steel-arch bridge. Journal of Bridge Engineering, 2019, 5(24): 05019004
20. Shao Y, Sun Z, Chen Y. Study on equal stiffness design of arch bridge suspenders and its dynamic response analysis. Journal of Vibration and Shock, 2018, 4(37): 219–225
21. Shao Y, Sun Z G, Chen Y F. Analysis of the impact effect of the suspender system in a half-through concrete filled steel tubular arch bridge. Applied Mechanics and Materials, 2013, 477–478: 705–709
22. Zhu J, Yi Q. Non-uniformity of stress impact factor of suspenders on half-through or through arch bridges. Journal of Vibration and Shock, 2012, 31(13): 5–10
23. Anitescu C, Atroshchenko E, Alajlan N. Artificial neural network methods for the solution of second order boundary value problems. Computers, Materials & Continua, 2019, 59(1): 345–359
24. Guo H, Zhuang X, Rabczuk T. A deep collocation method for the bending analysis of Kirchhoff Plate. Computers, Materials & Continua, 2019, 58(2): 433–456
25. Cai C S, Shi X M, Araujo M. Effect of approach span condition on vehicle-induced dynamic response of slab-on-girder road bridges. Engineering Structures, 2007, 29(12): 3210–3226
26. Zhang W, Cai C S, Pan F. Nonlinear fatigue damage assessment of existing bridges considering progressively deteriorated road conditions. Engineering Structures, 2013, 2013(56): 1922–1932
27. Kim B H, Park T. Estimation of cable tension force using the frequency-based system identification method. Journal of Sound and Vibration, 2007, 304(3–5): 660–676
28. Ren W X, Liu H L, Chen G. Determination of cable tensions based on frequency differences. Engineering Computations, 2008, 1(1): 172–189
29. Gan Q, Wang R, Rao R. Practical formula for estimation on the tensional force of cable by its measured natural frequencies. Chinese Journal of Theoretical and Applied Mechanics, 2010, 5(42): 983–987
30. He W. Study of suspender tension measurement based on frequency method with complex boundary conditions. China Civil Engineering Journal, 2012, 45(3): 93–98
31. Zhang W, Cai C S. Fatigue reliability assessment for existing bridges considering vehicle speed and road surface conditions. Journal of Bridge Engineering, 2012, 17(3): 443–453
32. Zhang W, Yuan H. Corrosion fatigue effects on life estimation of deteriorated bridges under vehicle impacts. Engineering Structures, 2014, 2014(71): 128–136
33. Hu P, Zhang C. Dynamic responses of bridge-embankment transitions in high speed railway: Field tests and data analyses. Engineering Structures, 2018, 175: 565–576
34. Yang H, He H, Zhang X, Yan W. Displacement dependent damping model for RC structure damage evolution and parameter identification method. Engineering Mechanics, 2017, 34(11): 126–134
35. Chen Y, Qian Y, Li H, He H. Damage detection and tests for a RC simply supported girder bridge based on its damping characteristics. Journal of Vibration & Shock, 2017, 36(13): 208–213
36. AASHTO. Manual for bridge evaluation. Washington D.C.: American Association of State Highway and Transportation Officials, 2011
37. TRB. Manual for bridge rating through load testing. Washington D.C.: Transportation Research Board, 1998
38. MOT. Code for Design of Highway Reinforced Concrete and Prestressed Concrete Bridges and Culverts. Beijing: Ministry of Transport of the People's Republic of China, 2004
39. Huang N E, Zheng S, Long S R. The empirical mode decomposition and the hilbert spectrum for nonlinear and non-stationary time series analysis. Proceedings Mathematical Physical and Engineering Sciences, 1971, 1998(454): 903–995
40. Yang Y B, Chang K C. Filtering techniques for extracting bridge frequencies from a test vehicle moving over the bridge. Engineering Structures, 2013, 2013(48): 353–362
41. Chen J, Xu Y. Application of HHT for modal parameter identification to civil structures. Journal of Vibration Engineering, 2003, 16(3): 383–388
42. Yang J X, Chen W Z, Rui G U. Analysis of dynamic characteristics of short hangers of arch bridge. Bridge Construction, 2014, 44(3): 13–18